JACS Au
AN OPEN ACCESS JOURNAL OF THE AMERICAN CHEMICAL SOCIETY

pubs.acs.org/jacsau
Letter

The Transformation Mechanism of Graphite to Hexagonal Diamond under Shock Conditions

Gu-Wen Chen, Sheng-Cai Zhu,* Liang Xu, Yao-Min Li, Zhi-Pan Liu,* Yanglong Hou,* and Ho-kwang Mao

Cite This: *JACS Au* 2024, 4, 3413−3420

Read Online

ACCESS | Metrics & More | Article Recommendations | Supporting Information

ABSTRACT: The formation of a hexagonal diamond represents one of the most intriguing questions in materials science. Under shock conditions, the graphite basal plane tends to slide and pucker to form diamond. However, how the shock strength determines the phase selectivity remains unclear. In this work, using a DFT-trained carbon global neural network model, we studied the shock-induced graphite transition. The poor sliding caused by scarce sliding time under high-strength shock leads to metastable hexagonal diamond with an orientation relationship of $(001)_G//(100)_{HD}+[010]_G//[010]_{HD}$, while under low-strength shock due to long sliding distance cubic diamond forms with the orientation $(001)_G//(111)_{CD}+[100]_G//[110]_{CD}$, unveiling the strength-dependent graphite transition mechanism. We for the first time provide computational evidence of the strength-dependent graphite transition from first-principles, clarifying the long-term unresolved shock-induced hexagonal diamond formation mechanism and the structural source of the strength-dependent trend, which facilitates the hexagonal diamond synthesis via controlled experiment.

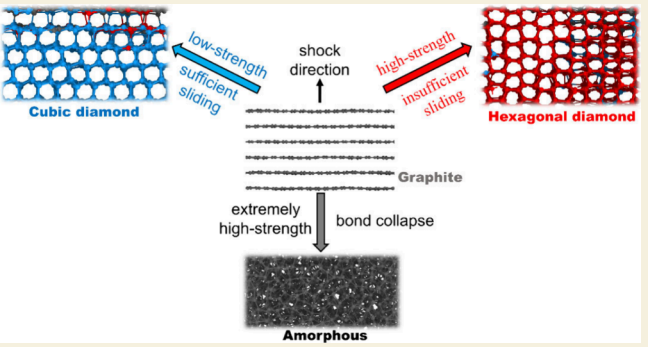

KEYWORDS: *hexagonal diamond, graphite, shock, molecular dynamics, neural network potential*

Four-coordinated carbon allotropes (sp^3-bonded), such as diamond, exhibit the highest hardness and illustrate excellent potential for technological applications. Over the past decades, multiple new sp^3-bonded carbon allotropes have been discovered and synthesized by well-developed techniques,[1−5] contributing to both scientific research and industrial applications. Lonsdaleite, however, has remained a mystic exception since 1962 when it was first proposed.[6] Lonsdaleite, also called hexagonal diamond (HD), was first found in the Canyon Diablo meteorite.[7] The shock-induced transition of graphite during meteorite impacts on both extraterrestrial bodies and Earth is believed to account for Lonsdaleite's formation, which could serve as marker for meteor impacts and the related aftermath.[8−11] Lonsdaleite has been attracting intense scientific interest in material science due to the potential superior mechanical properties.[12,13] Theoretical simulations[14] indicated that the hardness of HD may surpass cubic diamond (CD), the hardest materials in nature. Therefore, the experimental synthesis of HD from other carbon allotropes (particularly graphite) has been of practical and fundamental importance.

The challenge of synthesizing HD intrinsically originates from its thermodynamic metastability, since CD is the most thermodynamically stable high-pressure phase.[15] Consequently, only the kinetic-controlled approach is promising for the synthesis of HD, which demands stringent synthetic conditions. In 1960s, Bundy et al. first reported the experimental synthesis of hexagonal diamond at high-pressure and high-temperature (HPHT) conditions.[16] However, in subsequent decades, numerous HTHP experimental results have yielded only hexagonal diamond as a minority phase using various high-pressure techniques. The reported HD was identified mainly based on ambiguous X-ray diffraction (XRD) patterns or selected area electron diffraction due to the difficulty of synthesizing a bulk pure HD crystal.[17−20] Thus, the existence of HD has been under intense debate.[10,11,21,22] Some groups argued that the observation of HD in previous experiments and meteorites is merely a misinterpretation of defectivation of CD, and the HD cannot exist as an independent phase but only stacking fault or twins in CD.[10]

On the other hand, shock compression techniques that simulate meteorite impact have made desirable progress in HD

Received: June 20, 2024
Revised: August 9, 2024
Accepted: August 20, 2024
Published: August 25, 2024

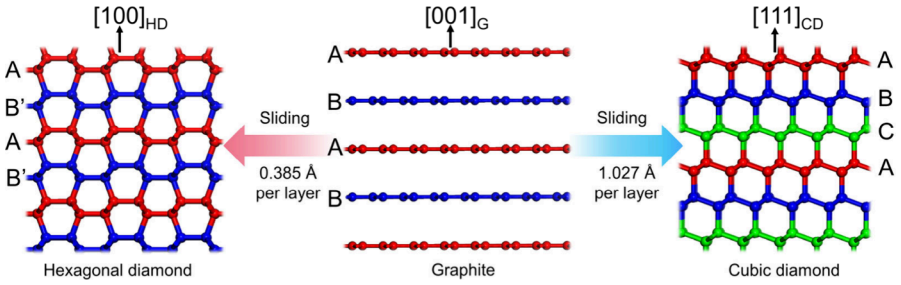

Figure 1. Orientation relation of graphite and shock-induced diamond.

synthesis. In the earlier 1990s, Erskine et al. reported the shock-induced martensitic transition with two-wave pattern from highly oriented graphite to CD with onset pressure of ∼19.6 GPa, which is overdriven to single-wave pattern above 40 GPa.[23,24] In subsequent decades, CD dominated the recover materials of most shock experiments.[25,26] Until recent years, using *in situ* XRD, Kraus[27] and Turneaure[28] et al. reported the shock-induced formation of HD from highly oriented pyrolytic graphite (HOPG). The discrepancy among these experiments indicates that the shock-induced transition of graphite possesses shock strength (evaluated by stress or particle velocity) selectivity, while the origin of shock strength selectivity has been unexplored until now. In addition, though such experimental efforts confirmed the possibility of HD synthesis from shock-compressed graphite, the critical shock strength for HD formation is still obscure. Kraus et al.[27] yielded HD with shock stress above 170 GPa, and Turneaure et al.[28] reported the HD formation at stress as low as ∼50 GPa, while Armstrong et al.[29] observed G/HD transition at a shock pressure of ∼80 GPa. The ambiguous conditions for HD formation not only hinder the synthesis of HD, but also possibly introduce incorrect interpretations of meteorite impact events. According to the orientation relation of transitional products from graphite (Figure 1), transverse layer sliding is a necessary stage during the transition from graphite to diamond. From a topological perspective, the layer sliding distances for G/CD and G/HD transitions are different. For the G/CD transition, a longer distance (at least 1.027 Å per layer) is needed from ABAB stacking to ABCABC stacking, while for the G/HD transition, a shorter distance (0.385 Å per layer) is needed from ABAB to AB'AB' stacking.

Theoretical simulations have been conducted extensively in recent years as an important step toward understanding the microscopic nature of graphite phase transition selectivity under shock. Via static simulation, some researchers[30−32] reported that graphite to CD has the lowest energy barrier, while some[33−35] reported that graphite to HD has the lowest energy barrier. In those static calculations, the energy barrier unit is eV/atom, not the true nucleation energy unit eV for the small periodic conditions cannot contain the true diamond nucleus inside. On the other hand, static simulations fail to simulate nonequilibrium process well, large-scale molecular dynamics (MD) simulations[36−39] are more efficacious to follow the shock-induced transition in real time. Via *ab initio* molecular dynamics simulation, Mundy et al.[38] found that graphite transforms to an intermediate layered diamond before it transforms into cubic diamond under shock. While integrating classical adaptive intermolecular reactive empirical bond order-Morse (AIREBO-M)[39] and long-range carbon bond-order potential II (LCBOPII)[37] potentials, Sun and Pineau found that graphite only yields CD as the main product regardless of the shock strength, with HD appearing as the twin structure. These results are inconsistent with the experimental findings. Unfortunately, to date, neither *ab initio*[38] nor empirical force field simulations[37,39] can reproduce the experimental shock-induced HD formation.[27,28] The *ab initio* simulations cannot reproduce the anisotropy of the graphite system due to the limited system size and high computational cost, while classical force fields are too simple in functional forms to capture the interatomic interactions of carbon since they are parametrized to match limited experimental thermophysical data and fail to reach the requisite accuracy. Even a more complex angular-dependent potential (ADP),[40] which was parametrized recently based on *ab initio* calculations by extending the multipole expansion approach to the quadrupole term, still fails to reproduce pure HD formation under high-strength shock (Supplementary Figure 5). Thus far, no conclusive computational evidence of the shock strength-dependent formation of pure HD is available, and an effective method that can identified between accuracy and speed is urgently needed to discover the shock-induced HD formation mechanism.

Recently, machine-learning (ML)-based atomic simulations have emerged as a major step forward for accelerating material research, which relies on predictive surrogate ML models, such as artificial neural networks (ANNs), to evaluate the atomic energy and force of complex potential energy surfaces (PESs). The neural network (NN) models can meet the needed level of accuracy and properly describe chemical reactions by pretraining a large representative PES data set calculated from quantum mechanics, from which the NN models capture the many-body correlations and complex polarizability effects of multidimensional PESs. The method pushes the boundaries of atomic simulations to a vast array of complex material and chemical reaction systems,[34,41] showing great advantages compared with classical force field methods in representativity, extensity, and continuity.[42] In this study, by using an *ab initio*-based global neural network (GNN) model of carbon trained on a density functional theory (DFT)-based PES data set globally sampled from stochastic surface walking (SSW) simulations,[43] we performed unbiased MD simulations to study the strength-dependent graphite-to-diamond phase transition mechanism under shock condition. By varying the particle velocities from 1.0 to 8.0 km/s, we found that graphite transforms into CD at velocities of 3.5−4.5 km/s, into HD at velocities above 4.5 km/s with an orientation relation of $(001)_G//(100)_{HD}$+$[010]_G//[010]_{HD}$, and into an amorphous carbon/HD phase at velocities above 6.0 km/s. Our simulations are uniquely consistent with the experimental shock-induced formation of HD and reveal the microstructural origin of the strength-dependent transition in graphite shock experiments. The proposed transition mechanism provides a

https://doi.org/10.1021/jacsau.4c00523
JACS Au 2024, 4, 3413−3420

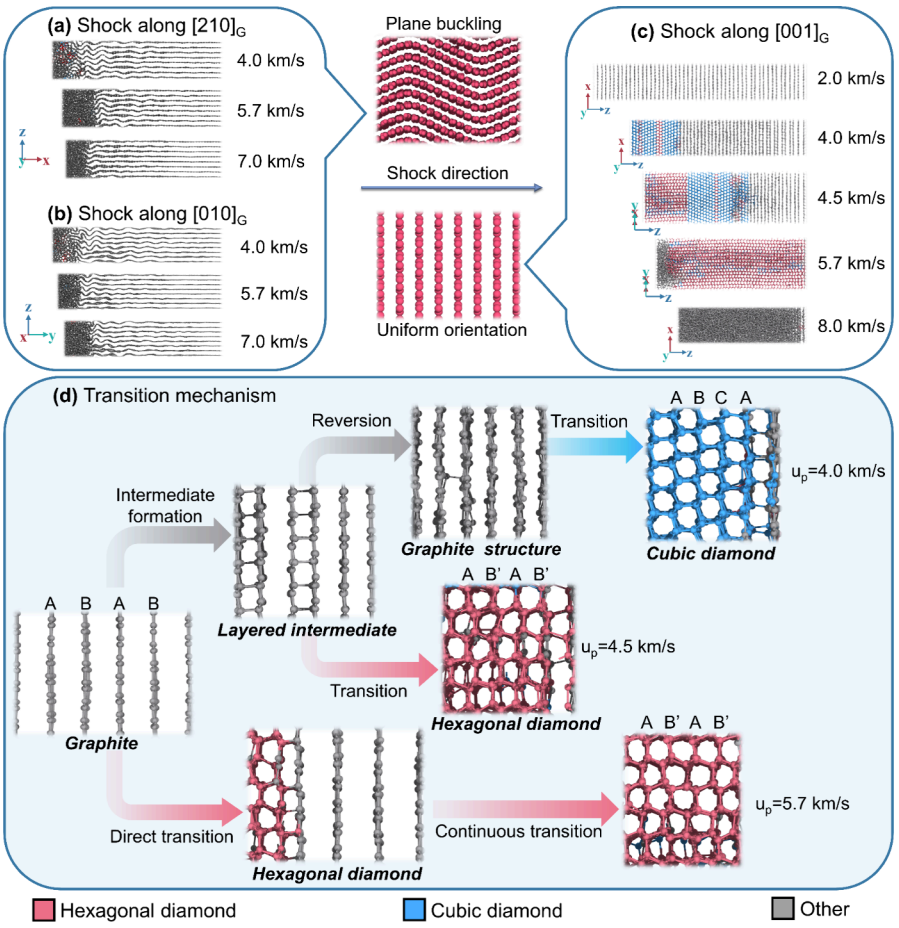

Figure 2. Shock simulation results along the (a) $[210]_G$ direction, (b) $[010]_G$ direction, and (c) $[001]_G$ direction. (d) Strength-dependent transition mechanism. Light red atoms represent the hexagonal diamond phase, light blue atoms represent the cubic diamond phase, and gray atoms represent either the graphite or amorphous phase.

basis for HD identification and, therefore, helps to further determine the critical shock strength to HD.

RESULTS AND DISCUSSION

The details of the GNN potential can be found in the Methods section. The benchmarks for the accuracy of this potential are presented in Supplementary Figure 1 and Supplementary Table 1, showing values comparable to those of DFT calculations. The shock MD simulations are performed in the large-scale atomic/molecular massively parallel simulator (LAMMPS) package,[44] and a detailed simulation method is presented in the Methods section. To rule out possible sizing effects caused by the periodic boundary conditions, we constructed a series of models with different sizes for shock simulations containing 1040, 4480, 7200, 9720, 10560, and 13728 atoms. For models with more than 9720 atoms, the simulation results show no significant difference, indicating that the system size is sufficiently large to obtain reliable results. We chose the simulation results of 13728 atoms (2.57 nm × 2.72 nm in the $x-y$ plane, 50 layers) for detailed analysis. To eliminate the synergistic interaction of incident and reflected shockwaves,[39] we only focus on the simulation time before shockwave reaching the box bottom. Shock simulations along the $[210]_G$ and $[010]_G$ directions were performed but only cause a zigzag-like bending of the graphite sheets, leading to amorphization (Figure 2a and b). Thus, in this work, we only focus on the shock simulations along the $[001]_G$ direction.

The main shock product structures of different particle velocities (u_p) along the $[001]_G$ direction are presented in Figure 2c. Other shocked structures and the structural evolution findings from simulations are shown in Supplementary Figures 2 and 3, respectively. The evolutions of temperature distribution are exhibited in Supplementary Figure 4, which shows a temperature surge after shock for the kinetic energy converts into thermal energy. As shown in Figure 2c, only elastic compression occurs when u_p < 3.5 km/s without a transition. The interlayer spacing is compressed but the typical layered structure is retained without interlayer bonding. When u_p increases to 3.5 km/s, the G/CD transition is observed under ∼50 GPa, with the first CD layer emerging at ∼0.9 ps. The orientation between graphite and CD is $(001)_G//(111)_{CD}$ + $[100]_G//[110]_{CD}$ (Figure 2d). Twin structures can be found in some cases (Figure 2c). When the u_p > 4.8 km/s, metastable HD is the main transitional product with an orientation of $(001)_G//(100)_{HD}$ + $[010]_G//[010]_{HD}$ (Figure 2d). The first HD layer emerges at ∼0.3 ps, much shorter than that of CD. Defects and deformation are found in the HD phase. The crystal quality improves as the u_p increases until reaching 5.7 km/s. The details of the G/CD and G/HD transition mechanisms are presented in Figure 2d and are discussed in detail in the following section. Interestingly, a mixed CD-HD phase is found at u_p = 4.5 km/s with ∼80 GPa

https://doi.org/10.1021/jacsau.4c00523
JACS Au 2024, 4, 3413−3420

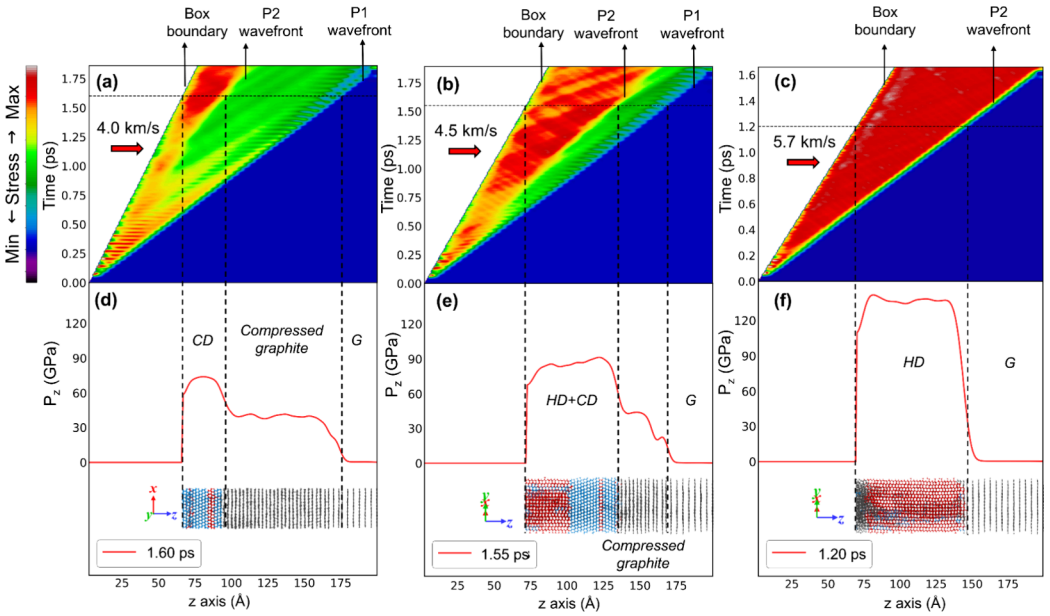

Figure 3. Layer-averaged longitudinal stress (P_z) analysis of three typical cases along the wave propagation direction. (a–c) Wavefront evolution with time. Red, green, and blue represent high, medium, and low stress, respectively. (d–f) Wave pattern and corresponding structural depiction at specific times. G: graphite, CD: cubic diamond; and HD, hexagonal diamond.

stress, which is the critical stress of HD formation in this study. When u_p reaches 7.0 km/s, graphite collapses structurally to an amorphous form due to the extremely high stress. Our simulations and the previous experimental results clearly show that the shock-induced transition of graphite is strength-dependent. For comparison, we performed similar simulations using other potentials (Supplementary Figure 5), including adp, edip, lcbop, and tersoff. Except for adp, which yields a small amount of HD at 4.0 km/s shock that returns to CD at 5.7 km/s shock, none of these empirical simulations can strictly reproduce the experimental shock-induced HD formation. To date, our *ab initio* NN simulations are uniquely consistent with previous experiments.[28]

To clarify the essence of this strength-dependent phenomenon, detailed shock stress (P_z) analysis was performed along the wave propagation direction for three typical cases. As shown in Figure 3a and d, a two-wave pattern is identified in the u_p = 4.0 km/s case, namely, the elastic wave (P1) and transitional wave (P2). P1 and P2 waves are integrated at first but gradually split into two waves (Figure 3a) because the P1 wave propagates much faster than the P2 wave. Under the P1 wave, the decreasing of interlayer spacing leads to the formation of a short-lived layered structure (Figure 2d) similar to that proposed by Mundy et al. in their *ab initio* study.[38] In this intermediate state, the graphite layers slide transversely, resulting in a slight stacking variation, but no obvious plane puckering is observed. The intermediate state lasts for ∼0.5 ps before reverting to the graphite structure with few interlayer bonds left (Figure 2d). When the P2 wave arrives, the graphite plane is bonded to the adjacent CD layer and puckers into a chair conformation. The graphite layer at the G/CD interface continues sliding to fit in the ABCA stacking and finally becomes a new CD layer (Figure 2d). The two-wave pattern accompanying CD formation is consistent with previous experimental results.[23,45] In this scenario, the simulation box is divided into three regions: uncompressed graphite, compressed graphite, and diamond (Figure 3d). Notably, there are some HD layers in the final CD matrix, resulting in twin structures.

Figure 3b and e shows the u_p = 4.5 km/s results, yielding an HD–CD mix product with a two-wave pattern. However, P1 is closer to P2 in this case than in the 4.0 km/s case. HD only forms in the early stage of shock, while CD formation follows HD formation (Figure 3e) after the separation of P1 and P2. Intriguingly, during the G/HD transition of this case, the layered intermediate structure directly transforms into HD (Figure 2d) instead of reverting to the graphite structure as the G/CD transition (similar to u_p = 4.0 km/s path in Figure 2d) shows.

Figure 3c and f shows the u_p = 5.7 km/s results with pure metastable HD phase formation. The wave profile and wavefront propagation analysis clearly show an overdriven single-wave pattern, consistent with previous experiments by Kraus et al.[27] and Turneaure et al.[28] Without the observation of the P1 wave, the short-lived layered structure is absent and the graphite directly transits into HD (Figure 2d). At the wavefront of the P2 wave, the graphite plane puckers into a boat configuration and is bonded with the adjacent HD layer to form the G/HD interface. Hindered by the interlayer bonds, the graphite layer in the interface slides only a short distance to fit in the AB'AB' stacking order. In this case, the simulation box is separated into two regions: uncompressed graphite and HD (Figure 3f). Notably, the amorphous phase forms in the early stage of the 5.7 km/s case, the amount of which increases with increasing particle velocity (Supplementary Figure 2).

We can find that the strength-dependent behavior has a strong relationship with the wave pattern and confirms the prevented sliding under a high-strength shock. With the two-wave pattern, the graphite layers can slide for a longer distance to fit the ABCA stacking, while with the single-wave pattern, the graphite layers only slide for a short distance to fit in the AB'AB' stacking. To further reveal the origin of sliding prevention, we analyzed the coupling relation of sliding and layer spacing variation (Figure 4). We chose six continuous

https://doi.org/10.1021/jacsau.4c00523
JACS Au 2024, 4, 3413–3420

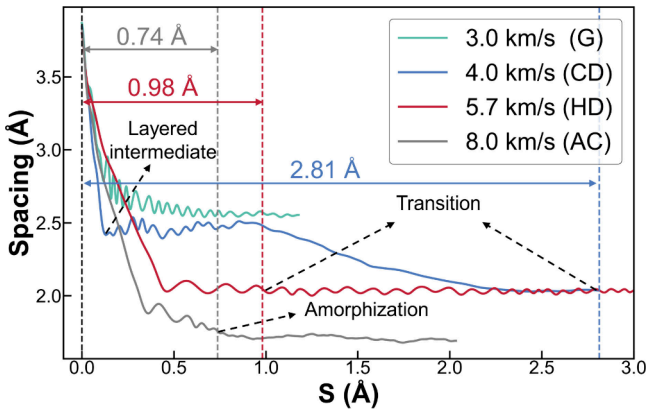

Figure 4. Spacing-sliding relation analysis. Conjoint analysis of u_p = 3.0, 4.0, 5.7, and 8.0 km/s. CD: cubic diamond, HD: hexagonal diamond, AC: amorphous carbon.

layers to evaluate their average spacing and centroid sliding in four cases. The centroid layer sliding distance (S^l) is defined by following equations:

$$\Delta S_x^l(t) = \frac{1}{N_l}\sum_i (X_i(t) - X_i(t-1)) \quad (1)$$

$$\Delta S_y^l(t) = \frac{1}{N_l}\sum_i (Y_i(t) - Y_i(t-1)) \quad (2)$$

$$\Delta S^l(t) = \sqrt{\Delta S_x^2(t) + \Delta S_y^2(t)} \quad (3)$$

$$S^l(t) = \sum_{t=0}^{t} \Delta S^l(t) \quad (4)$$

where l is the layer index, i represents the summation of all atoms in one layer, N is the quantity of atoms in one layer, and t represents the time. The parameter S^l is averaged by layer to obtain the parameter S. A larger value of S indicates a larger layer sliding distance.

Figure 4 compares the sliding-spacing evolution of u_p = 3.0 km/s (yielding compressed graphite), u_p = 4.0 km/s (yielding CD), u_p = 5.7 km/s (yielding HD), and u_p = 8.0 km/s (yielding amorphous carbon) cases. In the u_p = 3.0 km/s case, the interlayer spacing decreases to ∼2.6 Å under shock without transition for the large interlayer spacing. In the u_p = 4.0 km/s case, the process is divided into two steps. In the first step, the interlayer spacing decreases drastically until it reaches ∼2.5 Å, forming a layered intermediate via interlayer C−C bonds, while the sliding distance continuously increases. This step corresponds to the elastic wave. In the second step, the interlayer spacing resumes a slower decreasing trend and finally holds at ∼2.1 Å, meaning the transition completes with the per layer sliding distance reaching ∼2.81 Å. This step corresponds to the transitional wave. In contrast, in the u_p = 5.7 km/s case, the spacing directly decreases to ∼2.1 Å without standstill. For the interlayer C−C bond, the layer sliding distance is only ∼0.98 Å when the transition completes. In u_p = 8.0 km/s case, for the scarce sliding time, the sliding distance is only ∼0.74 Å while the interlayer spacing decreases to 1.8 Å, shorter than interlayer of CD(111) and HD(100) plane (∼2.1 Å), resulting amorphization.

The above analysis indicates that under low-strength shock the low stress induced by elastic wave, resulting in long sliding distance and subsequent CD formation, while under high-strength shock the single transitional wave induces rapid interlayer C−C bonding that leads to HD formation for insufficient sliding. To further confirm our arguments, shock simulation on randomly stacked graphite was conducted (Supplementary Figure 6), where the sliding advantage of HD formation is absent. This simulation yields CD as the only product regardless of the shock strength, and the sliding distance makes no difference to product type but only affects the product structure (Supplementary Figure 7), strongly confirming our conclusions. Our results quantitively agree with the speculation of Kraus et al.,[27] who considered that the sliding of graphite basal planes and CD formation can be prevented under high-strength shock conditions.

In this work, we found that shock strength determines the shock transition result; namely, high strength shock leads to HD formation, while low strength shock leads to CD formation, which agrees well with the experiments of Erskine,[23,24] Turneaure,[28] and Stavrou[35] et al. Under low-strength shock pressure of 20−40 GPa, Erskine et al.[23,24] observed CD formation from graphite with two-wave pattern; while under high-strength shock pressure above 50 GPa, Turneaure[28] and Stavrou et al.[35] observed HD formation with single-wave pattern. However, our results do not fully consist with Kraus et al. results,[27] who found that graphite transits to CD under 50−170 GPa with single-wave pattern. Our simulation results show that the overdriven single-wave pattern implies prevented sliding and favors HD formation. Such discrepancies would be for the fairly limited diffraction data (one peak for CD and only two peaks for HD, with all three peaks located at similar scattering angles) to identify the product phases, as Turneaure[28] pointed out. This work reveals that the coupling relation of interlayer-spacing and layer-sliding is the cornerstone of the shock-strength-dependent phenomenon, and the overdriven single-wave pattern may imply the HD formation in the shock experiment. The proposed mechanism provides an identification the basis of the wave pattern for HD formation in shock experiments, helping to further determine the critical shock strength for HD formation.

In addition, from the atomic mechanism of graphite to HD, we can find that the stress direction and the graphite basal plane sliding play key roles in HD formation. Our simulations show that shock along the $[210]_G$ and $[010]_G$ directions causes a zigzag-like bending of the graphite sheets. Consequently, the HD cannot form in such condition for the change of the graphite basal plane sequence. While under shock along the $[001]_G$ direction, the shock strength determines the HD formation, namely, long sliding distance induces CD formation while short sliding distance induces HD formation. Thus, it should keep the graphite basal plane flat and inhibit its sliding to synthesize the HD in the hydrostatic experiment. Thus, compression on graphite along $[001]_G$ would be a reasonable way to keep the graphite basal plane flat, and mild temperature is recommended to be used to overcome the barrier but inhibit the graphite basal plane sliding.

CONCLUSION

In summary, by using an *ab initio* NN model of carbon, our unbiased shock simulations of hexagonal graphite uniquely reproduce the previous experimental results and reveal the structural origin of the shock-strength-dependent transition. The G/CD transition is observed at particle velocities above 3.5 km/s via a diffusion-free process. The G/HD transition

https://doi.org/10.1021/jacsau.4c00523
JACS Au 2024, 4, 3413−3420

occurs at particle velocities above 4.5 km/s. Evident amorphization is found at particle velocities above 6.0 km/s. The coupling relation of interlayer spacing and layer sliding are the cornerstone of the strength-dependent phenomenon. In low-strength shock cases with a two-wave pattern, sufficient sliding time leads to a long sliding distance, favoring CD formation. Conversely, in high-strength shock cases with an overdriven single-wave pattern, insufficient layer sliding leads to a metastable HD phase. Extremely high-strength shock may induce bond collapse and consequent amorphization. Our study not only reveals the long-term unresolved shock-induced HD formation mechanism but also provides a HD synthesis method, namely, inhibiting the graphite basal plane sliding via controlled experiments.

METHODS

Molecular Dynamics Simulation

In this paper, all simulations were performed on Large-scale Atomic/Molecular Massively Parallel Simulator (LAMMPS) package[44] with the carbon NN potential. We built quasi-1D samples whose longitudinal size (along $[001]_G$) is larger than the transverse sizes with different atomic quantities (containing 1040, 4480, 7200, 9720, 10560, and 13728 atoms, respectively) to carry out convergence test. In every test, carbon atoms were first assigned with initial velocities according to a Gaussian distribution at T = 300 K, and then thermally equilibrated in the isothermal−isobaric (NPT) ensemble at a pressure of 0 MPa for 20 ps with time step set to be 1 fs. We set periodic boundary conditions along all axes during equilibration. For the shock simulation, a vacuum with ∼50 Å thickness was added to the graphite model. The first layer of graphite was assigned a constant atomic velocity along the z axis (namely, the shock particle velocity u_p) while velocities of x and y were set to be 0, acting as a piston. And all force on the first layer was removed. The last layer was fixed by the same setting except for velocity along z axis also set to be 0. Following analysis would leave out these two layers for strictness. Shock simulations were conducted in the NVE ensemble with a time step of 0.1 fs and for a time sufficiently long to ensure the wavefront reaching the bottom of the box. We only focused on the time before wavefront reaching the box bottom. In convergence test, the particle velocity was fixed to be 5.0 km/s. For models with atom number exceeding 9720, the simulation results showed no significant difference, indicating that the results had been convergent. We chose the model with 13728 atoms for subsequent simulations and analysis for a wide range of particle velocities (1.0 to 8.0 km/s). To clarify the effect of shock direction, we also performed similar shock simulations on $[210]_G$ and $[010]_G$, where the longitudinal directions of quasi-1D samples are along $[210]_G$ and $[010]_G$, respectively.

The simulation results were visualized with OVITO.[46] To observe the interlayer bonds, the cutoff distance was set as 1.6 Å, which is close to the representative bond length of sp^3-sp^3 carbon atoms (1.54 Å). Local structural analysis was performed by Identify diamond structure modification implemented in the OVITO software.

GNN Parameters

The GNN potential is generated by SSW-NN method,[43] which is now implemented in the LASP software.[47] The NN follows the feed-forward NN architecture with five layers (210−90−80−80−5), reaching 62019 fitting parameters, within 173 two-body and 37 three-body descriptors. With great representativity, the DFT training data set contains 62019 structures, including 1299 clusters, 5857 layer structures, and 54863 bulk structures (Supplementary Table 2). For the final NN potential, the root-mean-square (RMS) errors for the energy, force, and stress reaches 9.311 meV/atom, 0.231 eV/Å, and 3.959 GPa, respectively.

Stress Analysis

The per-atom pressure tensor (or compressive stress) was computed by eq 5:

$$P_{i\alpha\beta}V_\alpha = m_i v_{i\alpha} v_{i\beta} + \frac{1}{2}\sum_j (r_{i\alpha}F_{i\beta} + r_{j\alpha}F_{j\beta}) \quad (5)$$

where α and β take on values x, y, and z, m_i is the atomic mass, and V_α is the atomic volume. The first term of eq 5 represents the momentum flow of atom i, while the last terms correspond to the virial due to the pairwise interaction of atom i situated at position r_i with atom j at position r_j. F_i and F_j are, respectively, forces on atoms i and j, while the latter sums over all neighbors of atom i. Then, the individual atomic volume was estimated by using the Voronoi tessellation method with the VORO++ package. To display the wave profile, the longitudinal pressure P_z was averaged in every layer.

ASSOCIATED CONTENT

Supporting Information

The Supporting Information is available free of charge at https://pubs.acs.org/doi/10.1021/jacsau.4c00523.

NN potential accuracy benchmarks, components of the NN training data set, shocked product structures, structural evolution characteristics of simulations, simulation results with other potentials, simulation results of randomly stacked graphite, and spacing-sliding relation analysis on randomly stacked graphite (PDF)

AUTHOR INFORMATION

Corresponding Authors

Sheng-Cai Zhu − *School of Materials, Shenzhen Campus of Sun Yat-sen University, Shenzhen 518107, China;* orcid.org/0000-0003-3311-6723; Email: zhushc@mail.sysu.edu.cn

Zhi-Pan Liu − *Collaborative Innovation Center of Chemistry for Energy Material, Shanghai Key Laboratory of Molecular Catalysis and Innovative Materials, Key Laboratory of Computational Physical Science, Department of Chemistry, Fudan University, Shanghai 200433, China;* orcid.org/0000-0002-2906-5217; Email: zpliu@fudan.edu.cn

Yanglong Hou − *School of Materials, Shenzhen Campus of Sun Yat-sen University, Shenzhen 518107, China;* orcid.org/0000-0003-0579-4594; Email: hou@pku.edu.cn

Authors

Gu-Wen Chen − *School of Materials, Shenzhen Campus of Sun Yat-sen University, Shenzhen 518107, China*

Liang Xu − *National Key Laboratory of Shock Wave and Detonation Physics, Institute of Fluid Physics, China Academy of Engineering Physics, Mianyang 621900, China*

Yao-Min Li − *College of Aerospace Engineering, Nanjing University of Aeronautics and Astronautics, Nanjing 210016, China*

https://doi.org/10.1021/jacsau.4c00523
JACS Au 2024, 4, 3413−3420

Ho-kwang Mao − *Center for High Pressure Science and Technology Advanced Research (HPSTAR), Beijing 100094, China*

Complete contact information is available at: https://pubs.acs.org/10.1021/jacsau.4c00523

Author Contributions

S.Z. conceived the research idea and organized the collaboration. S.Z., Y.H., and Z.L. supervised the work. G.C. and S.Z. designed the simulations and prepared the manuscript. G.C. and S.Z. conducted the simulations and analysis work. Y.L. assisted with simulations. Y.H., H.M., Z.L., and L.X. contributed to the revision of the manuscript.

Funding

This work was supported by the National Science Foundation of China (Grant Nos. 12274383, 92263203, 52027801) and Fundamental Research Funds for the Central Universities, Sun Yat-sen University (Grant No. 23qnpy04), National Key Research and Development Program of China (No. 2022YFA1203902, No. 2022YFA1200093).

Notes

The authors declare no competing financial interest.

■ ACKNOWLEDGMENTS

We acknowledge the use of computing resources from the Tianhe-2 Supercomputer.

■ REFERENCES

(1) Li, Q.; Ma, Y.; Oganov, A. R.; et al. Superhard Monoclinic Polymorph of Carbon. *Phys. Rev. Lett.* **2009**, *102*, No. 175506.
(2) Umemoto, K.; Wentzcovitch, R. M.; Saito, S.; et al. Body-Centered Tetragonal C_4: A Viable sp^3 Carbon Allotrope. *Phys. Rev. Lett.* **2010**, *104*, No. 125504.
(3) Wang, J.-T.; Chen, C.; Kawazoe, Y. Low-Temperature Phase Transformation from Graphite to Sp3 Orthorhombic Carbon. *Phys. Rev. Lett.* **2011**, *106*, No. 075501.
(4) Zhao, Z.; Xu, B.; Zhou, X.-F.; et al. Novel Superhard Carbon: C-Centered Orthorhombic C8. *Phys. Rev. Lett.* **2011**, *107*, No. 215502.
(5) Shang, Y.; Liu, Z.; Dong, J.; et al. Ultrahard bulk amorphous carbon from collapsed fullerene. *Nature* **2021**, *599*, 599−604.
(6) ERGUN, S.; ALEXANDER, L. E. Crystalline Forms of Carbon: A Possible Hexagonal Polymorph of Diamond. *Nature* **1962**, *195*, 765−7.
(7) Shumilova, T. G.; Mayer, E.; Isaenko, S. I. Natural monocrystalline lonsdaleite. *Dokl Earth Sci.* **2011**, *441*, 1552−4.
(8) Kennett, D. J.; Kennett, J. P.; West, A.; et al. Shock-synthesized hexagonal diamonds in Younger Dryas boundary sediments. *Proc. Natl. Acad. Sci. U.S.A* **2009**, *106*, 12623−8.
(9) Carlisle, D. B.; Braman, D. R. Nanometre-size diamonds in the Cretaceous/Tertiary boundary clay of Alberta. *Nature* **1991**, *352*, 708−9.
(10) Németh, P.; Garvie, L. A. J.; Aoki, T.; et al. Lonsdaleite is faulted and twinned cubic diamond and does not exist as a discrete material. *Nat. Commun.* **2014**, *5*, 5447.
(11) Salzmann, C. G.; Murray, B. J.; Shephard, J. J. Extent of stacking disorder in diamond. *Diam Relat Mater.* **2015**, *59*, 69−72.
(12) Güler, E.; Güler, M. Elastic and mechanical properties of hexagonal diamond under pressure. *Appl. Phys. A: Mater. Sci. Process.* **2015**, *119*, 721−6.
(13) Volz, T. J.; Gupta, Y. M. Elastic moduli of hexagonal diamond and cubic diamond formed under shock compression. *Phys. Rev. B* **2021**, *103*, No. L100101.
(14) Pan, Z.; Sun, H.; Zhang, Y.; et al. Harder than Diamond: Superior Indentation Strength of Wurtzite BN and Lonsdaleite. *Phys. Rev. Lett.* **2009**, *102*, No. 055503.
(15) He, C.; Sun, L.; Zhang, C.; et al. Four superhard carbon allotropes: a first-principles study. *Phys. Chem. Chem. Phys.* **2012**, *14*, 8410.
(16) Bundy, F. P.; Kasper, J. S. Hexagonal Diamond—A New Form of Carbon. *J. Chem. Phys.* **1967**, *46*, 3437−46.
(17) Yoshiasa, A.; Murai, Y.; Ohtaka, O.; et al. Detailed Structures of Hexagonal Diamond (lonsdaleite) and Wurtzite-type BN. *Jpn. J. Appl. Phys.* **2003**, *42*, 1694−704.
(18) Kulnitskiy, B.; Perezhogin, I.; Dubitsky, G.; et al. Polytypes and twins in the diamond−lonsdaleite system formed by high-pressure and high-temperature treatment of graphite. *Acta Crystallogr. B Struct Sci. Cryst. Eng. Mater.* **2013**, *69*, 474−9.
(19) Isobe, F.; Ohfuji, H.; Sumiya, H.; Irifune, T. Nanolayered Diamond Sintered Compact Obtained by Direct Conversion from Highly Oriented Graphite under High Pressure and High Temperature. *J. Nanomater* **2013**, *2013*, 1−6.
(20) Shiell, T. B.; McCulloch, D. G.; Bradby, J. E.; Haberl, B.; Boehler, R.; McKenzie, D. R. Nanocrystalline hexagonal diamond formed from glassy carbon. *Sci. Rep* **2016**, *6*, No. 37232.
(21) Jones, A. P.; McMillan, P. F.; Salzmann, C. G.; et al. Structural characterization of natural diamond shocked to 60 GPa; implications for Earth and planetary systems. *Lithos* **2016**, *265*, 214−21.
(22) Greshnyakov, V. A.; Belenkov, E. A.; Brzhezinskaya, M. M. Theoretical Investigation of Phase Transitions of Graphite and Cubic 3C Diamond Into Hexagonal 2H Diamond Under High Pressures. *Phys. Status Solidi (b)* **2019**, *256*, No. 1800575.
(23) Erskine, D. J.; Nellis, W. J. Shock-induced martensitic phase transformation of oriented graphite to diamond. *Nature* **1991**, *349*, 317−9.
(24) Erskine, D. J.; Nellis, W. J. Shock-induced martensitic transformation of highly oriented graphite to diamond. *J. Appl. Phys.* **1992**, *71*, 4882−6.
(25) Chen, P. W.; Ding, Y. S.; Chen, Q.; et al. Spherical nanometer-sized diamond obtained from detonation. *Diam Relat Mater.* **2000**, *9*, 1722−5.
(26) Chen, P.; Huang, F.; Yun, S. Characterization of the condensed carbon in detonation soot. *Carbon N Y* **2003**, *41*, 2093−9.
(27) Kraus, D.; Ravasio, A.; Gauthier, M.; et al. Nanosecond formation of diamond and lonsdaleite by shock compression of graphite. *Nat. Commun.* **2016**, *7*, No. 10970.
(28) Turneaure, S. J.; Sharma, S. M.; Volz, T. J.; Winey, J. M.; Gupta, Y. M. Transformation of shock-compressed graphite to hexagonal diamond in nanoseconds. *Sci. Adv.* **2017**, *3*, No. eaao3561.
(29) Armstrong, M. R.; Radousky, H. B.; Austin, R. A.; et al. Highly ordered graphite (HOPG) to hexagonal diamond (lonsdaleite) phase transition observed on picosecond time scales using ultrafast x-ray diffraction. *J. Appl. Phys.* **2022**, *132*, No. 055901.
(30) Dong, X.; Zhou, X.-F.; Qian, G.-R.; et al. An ab initio study on the transition paths from graphite to diamond under pressure. *J. Phys-condens Mat* **2013**, *25*, No. 145402.
(31) Greshnyakov, V. A.; Belenkov, E. A. Investigation on the formation of lonsdaleite from graphite. *J. Exp Theor Phys.* **2017**, *124*, 265−74.
(32) Tateyama, Y.; Ogitsu, T.; Kusakabe, K.; et al. Constant-pressure first-principles studies on the transition states of the graphite-diamond transformation. *Phys. Rev. B* **1996**, *54*, 14994−5001.
(33) Yang, X.; Dong, J.; Yao, M.; et al. Diamond-graphite nanocomposite synthesized from multi-walled carbon nanotubes fibers. *Carbon N Y* **2021**, *172*, 138−43.
(34) Xie, Y. P.; Zhang, X. J.; Liu, Z. P. Graphite to Diamond: Origin for Kinetics Selectivity. *J. Am. Chem. Soc.* **2017**, *139*, 2545−8.
(35) Stavrou, E.; Bagge-Hansen, M.; Hammons, J. A.; et al. Detonation-induced transformation of graphite to hexagonal diamond. *Phys. Rev. B* **2020**, *102*, No. 104116.

(36) Khaliullin, R. Z.; Eshet, H.; Kühne, T. D.; et al. Nucleation mechanism for the direct graphite-to-diamond phase transition. *Nat. Mater.* **2011**, *10*, 693−7.
(37) Pineau, N. Molecular dynamics simulations of shock compressed graphite. *J. Phys. Chem. C* **2013**, *117*, 12778−86.
(38) Mundy, C. J.; Curioni, A.; Goldman, N.; et al. Ultrafast transformation of graphite to diamond: An *ab initio* study of graphite under shock compression. *J. Chem. Phys.* **2008**, *128*, 425.
(39) Sun, H.; Jiang, X.; Dai, R.; et al. Understanding the mechanism of shockwave induced graphite-to-diamond phase transition. *Materialia* **2022**, *24*, No. 101487.
(40) Zhu, S.; Yan, X.; Liu, J.; et al. A Revisited Mechanism of the Graphite-to-Diamond Transition at High Temperature. *Matter* **2020**, *3*, 864−78.
(41) Kang, P.-L.; Shang, C.; Liu, Z.-P. Glucose to 5-Hydroxymethylfurfural: Origin of Site-Selectivity Resolved by Machine Learning Based Reaction Sampling. *J. Am. Chem. Soc.* **2019**, *141*, 20525−36.
(42) Kang, P. L.; Shang, C.; Liu, Z. P. Large-Scale Atomic Simulation via Machine Learning Potentials Constructed by Global Potential Energy Surface Exploration. *Acc. Chem. Res.* **2020**, *53*, 2119−29.
(43) Huang, S.-D.; Shang, C.; Zhang, X.-J.; et al. Material discovery by combining stochastic surface walking global optimization with a neural network. *Chem. Sci.* **2017**, *8*, 6327−37.
(44) Plimpton, S. Fast Parallel Algorithms for Short-Range Molecular Dynamics. *J. Comput. Phys.* **1995**, *117*, 1−19.
(45) Erskine, D. J.; Nellis, W. J. Shock-induced martensitic transformation of highly oriented graphite to diamond. *J. Appl. Phys.* **1992**, *71*, 4882−6.
(46) Stukowski, A. Visualization and analysis of atomistic simulation data with OVITO−the Open Visualization Tool. *Model Simul Mat Sci. Eng.* **2010**, *18*, No. 015012.
(47) Huang, S Da; Shang, C.; Kang, P. L.; et al. LASP: Fast global potential energy surface exploration. *Wiley Interdiscip Rev. Comput. Mol. Sci.* **2019**, *9*, 1−11.

https://doi.org/10.1021/jacsau.4c00523
JACS Au 2024, 4, 3413−3420